On the vibro-acoustic response of a cylindrical shell submerged near a free sea surface

Adrien Marsick, Gyani Shankar Sharma, Daniel Eggler, Laurent Maxit, Valentin Meyer, Nicole Kessissoglou

On the vibro-acoustic response of a cylindrical shell submerged near a free sea surface

Adrien Marsick,[1,2] Gyani Shankar Sharma,[2*] Daniel Eggler,[2] Laurent Maxit,[1] Valentin Meyer,[3] Nicole Kessissoglou[1]

[1]Univ Lyon, INSA Lyon, LVA , 25 bis, av. Jean Capelle, F-69621, Villeurbanne Cedex, France

[2]School of Mechanical and Manufacturing Engineering, UNSW Sydney, Australia

[3]Naval Group Research, 199 Avenue Pierre-Gilles de Gennes, 83190, Ollioules, France

*Email : gyanishankar.sharma@unsw.edu.au

Abstract

A vibro-acoustic model of a structurally excited cylindrical shell of infinite length submerged in a heavy fluid at a finite distance from a free surface is presented. Expressions for the shell displacement, the acoustic pressure in the interior cavity of the shell and the acoustic pressure at all field locations in the exterior domain are analytically derived. The formulation for the exterior acoustic pressure is developed using the image method and Graf's addition theorem. Results for the structural and acoustic responses of the cylindrical shell submerged at a finite distance from the free surface and in an unbounded fluid domain are compared. The effects of the shell circumferential modes, interior cavity resonances and proximity of the free surface on the shell acoustic responses are examined. New mechanisms influencing the low frequency vibro-acoustic response of a submerged hull near a fluid boundary are described.

1. Introduction

Vibro-acoustic analyses of fluid-loaded cylindrical shells are important for a broad range of applications including underwater vehicles, offshore pile driving and submarine cables. Heavy fluid loading from the surrounding water alters the dynamic characteristics of a submerged elastic shell. Prediction of the vibro-acoustic response of a fluid-loaded shell is a classic acoustic-structure interaction problem, for example, see [1–7]. At low frequencies, the heavy fluid can be approximated as an added mass loading on the structure. As the frequency increases, damping effects of the fluid must be taken into account. The vibro-acoustic response of an elastic shell submerged in an unbounded fluid domain has also been examined using numerical discretisation methods such as the finite element method and the boundary element method [8–11]. The in-vacuo modes no longer form the modal basis for an elastic structure submerged in a heavy fluid, necessitating computation of the wet structural modes [12].

For underwater vehicles navigating in shallow waters or where the fluid domain cannot be considered as unbounded, the influence of the free sea surface or seabed needs to be taken into account. Salaün [13] studied the effect of the free surface on the far-field pressure radiated by a semi-immersed cylindrical shell. The free surface was modelled by applying the pressure loading associated with the sea water to the wetted surface of the shell. A common approach to model the effect of the free surface for a fully immersed structure is the image method. The image method was first employed to study radiation of simple acoustic sources near a plane boundary, showing Lloyd's mirror behaviour for near-surface monopoles [14–18]. The image method has also been implemented to study sound scattering by a rigid cylinder near an impedance boundary, displaying similar patterns of enhanced or reduced scattering depending on the proximity to the planar surface [19–21]. More recently, the vibrational characteristics and far-field sound radiation of a cylindrical shell near an impedance plane or a free sea surface has been studied [22–26]. Li and co-authors [24,25] investigated the acoustic responses of cylindrical shells of infinite and finite length submerged at a finite depth from the free surface. The far-field sound was approximated using the method of stationary phase. The amplitude of the radiated sound was found to oscillate with variation of depth from the free surface and frequency. Close proximity to the free surface was also

observed to have a significant impact on the shell vibrational characteristics. Guo et al. [26] presented a hybrid analytical/numerical approach to obtain the vibro-acoustic response of a finite cylindrical shell submerged near a free surface. The shell vibrational responses derived analytically were used as an input to a boundary element model to numerically predict the far-field radiated sound. They showed that the vibro-acoustic response of the cylindrical shell submerged at a finite depth tends towards the response in an infinite domain when the submerged depth exceeds a certain value. In the aforementioned studies, the acoustic responses of a cylindrical shell submerged near a free surface were approximated using the method of stationary phase or numerical discretisation methods.

We present an analytical formulation to investigate the effect of a free sea surface on the vibro-acoustic response of an infinite cylindrical shell. Reflections from the free surface are estimated using the image method. The presence of an internal acoustic fluid in the cylindrical shell cavity is considered. The acoustic-structure interaction between the interior acoustic domain of the shell, its vibrational response and the exterior acoustic domain are simultaneously taken into account. Both the near-field and far-field acoustic responses of the cylindrical shell are predicted. The combined influence of the immersion depth and the shell structural and cavity resonances on its vibro-acoustic responses are observed. Insights into the physical mechanisms influencing the structural and acoustic responses of a submerged hull near a free surface are described.

2. Analytical formulation

2.1 Cylindrical shell submerged in a fluid of infinite extent

We consider an infinitely long, thin cylindrical shell, as shown in Fig. 1. The shell displacements in the longitudinal, tangential, and radial directions are denoted by u, v and w, respectively. The cylindrical shell has thickness h, mean radius a, complex Young's modulus E, Poisson's ratio ν and density ρ_s. The shell is submerged in a heavy fluid of density ρ_{ext} and speed of sound c_{ext}, where the subscript ext denotes the exterior fluid domain. The shell is also filled with an internal fluid of density ρ_{int} and speed of sound c_{int}, where the subscript int denotes the interior acoustic domain. The exterior and interior acoustic fields act as pressure loads on the cylindrical shell. Further, the cylinder is excited by a harmonic radial line force f at an angular position θ_f. The system is invariant under translation in the direction z. A harmonic dependency of $e^{-\mathrm{i}\omega t}$ has been assumed, where $\mathrm{i} = \sqrt{-1}$, where ω is the angular frequency and t is time. It should be noted that the analytical formulation considers a linear vibro-acoustic problem and as such, does not take into account the instability or buckling of the shell under hydrostatic pressure.

The exterior and interior acoustic pressures can be expressed in terms of a classic Fourier series as follows [27]

$$p_{\text{ext}}(r,\theta) = \sum_{n=-\infty}^{\infty} A_n \frac{H_n(k_{\text{ext}}r)}{H_n'(k_{\text{ext}}a)} e^{\mathrm{i}n\theta}, \tag{1}$$

$$p_{\text{int}}(r,\theta) = \sum_{n=-\infty}^{\infty} B_n \frac{J_n(k_{\text{int}}r)}{J_n'(k_{\text{int}}a)} e^{\mathrm{i}n\theta}, \tag{2}$$

where A_n, B_n are Fourier coefficients of order n, k_{ext}, k_{int} respectively denote the acoustic wavenumbers associated with the exterior and interior acoustic domains. H_n is the Hankel function of the first kind of order n and H_n' is its derivative with respect to the argument. Similarly, J_n is the Bessel of the first kind of order n and $J_n{}'$ is its derivative with respect to the argument.

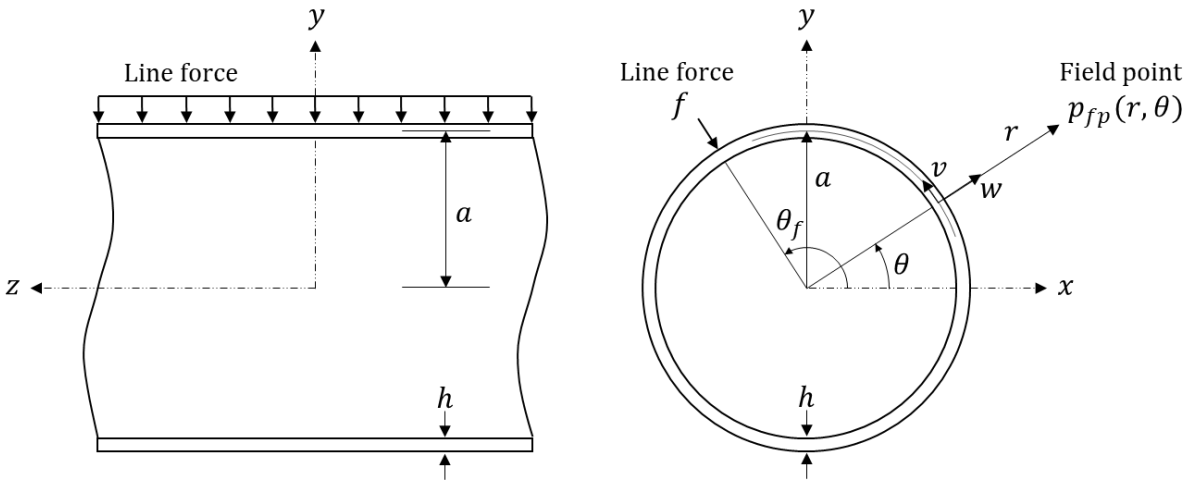

Fig. 1. Schematic diagram of the cylindrical shell excited by a line force and the coordinate system.

2.2 Cylindrical shell submerged beneath a free surface

The cylindrical shell is submerged at a finite depth d from a free surface. The free surface can be modelled as a flat pressure release surface due to high impedance mismatch between water and air [28]. The acoustic pressure at a field point is derived as the sum of the direct radiated pressure and the reflected pressure from the free surface, whereby the latter is modelled by introducing an image cylinder as shown in Fig. 2.

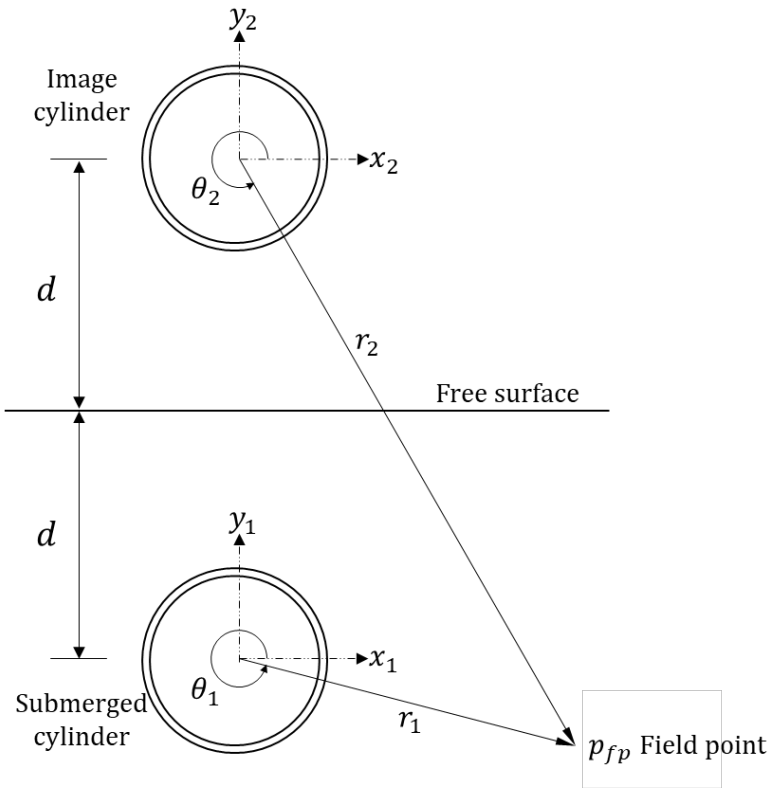

Fig. 2. Schematic diagram of the cylindrical shell submerged below the free surface and its image above the free surface, showing the local coordinate system for each cylindrical shell.

The total acoustic pressure p_{fp} at an external field point for the submerged cylindrical shell is given by the summation of the external pressure due to the submerged cylinder and its image, that is, $p_{fp} = p_1 + p_2$. Using Eq. (1), the acoustic pressures at a field point associated with the submerged and image cylindrical shells are given by

$$p_1(r_1, \theta_1) = \sum_{n=-\infty}^{\infty} A_{n,1} \frac{H_n(k_{\text{ext}} r_1)}{H_n'(k_{\text{ext}} a)} \, e^{\text{i}n\theta_1}, \tag{3}$$

$$p_2(r_2, \theta_2) = \sum_{n=-\infty}^{\infty} A_{n,2} \frac{H_n(k_{\text{ext}} r_2)}{H_n'(k_{\text{ext}} a)} \, e^{\text{i}n\theta_2}, \tag{4}$$

where the subscripts 1 and 2 respectively denote the submerged and image cylinders, and $A_{n,1}$, $A_{n,2}$ represent the corresponding Fourier coefficients for the exterior acoustic pressure.

In what follows, the total acoustic pressure at a field point is expressed in terms of the Fourier coefficients and local coordinate system of the submerged cylinder. First, boundary conditions at the free surface are used to represent the Fourier coefficients of the image cylinder in terms of the coefficients of the submerged cylinder. At the free surface boundary corresponding to $r_2 = r_1$ and $\theta_2 = 2\pi - \theta_1$, the total acoustic pressure is equal to zero, that is, $p_1 + p_2 = 0$. Substituting the geometric equalities in Eq. (4), employing the Hankel function property given by $H_{-n}(z) = (-1)^n H_n(z)$ [29], and equating the total pressure to zero, yields a relation between the Fourier coefficients of the submerged and image cylinders given by $A_{n,2} = -A_{-n,1}$. Graf's addition theorem is then employed to convert the local coordinate system of the image cylinder to that of the submerged cylinder. Applying Graf's addition theorem in the vicinity of the submerged cylinder ($r_1 < 2d$), the Hankel function associated with the image cylinder becomes [27]

$$H_n(k_{\text{ext}} r_2) e^{\text{i}n\theta_2} = \sum_{m=-\infty}^{\infty} H_{n-m}\,(2k_{\text{ext}} d) J_m(k_{\text{ext}} r_1) e^{\text{i}m\theta_1}. \tag{5}$$

It should be noted that the use of Graf's addition theorem introduces an error in the estimation of the exterior pressure at $r_1 = 2d$, as highlighted in [30]. Substituting Eq. (5) into Eq. (4) and employing the Hankel function relation $H_{-n}(z)$ yields an expression for the acoustic pressure of the image cylinder in terms of the local coordinate system of the submerged cylinder as follows

$$p_2(r_1, \theta_1) = -\sum_{n=-\infty}^{\infty} \sum_{m=-\infty}^{\infty} (-1)^m A_{n,1} \frac{H_{n+m}\,(2k_{\text{ext}} d) J_m(k_{\text{ext}} r_1)}{H_n'(k_{\text{ext}} a)} e^{\text{i}m\theta_1}. \tag{6}$$

Exchanging the order of m and n in Eq. (6) and using Eq. (3), the total acoustic pressure for a submerged cylinder taking into account reflections from the free surface becomes

$$p_{fp}(r_1, \theta_1) = \sum_{n=-\infty}^{\infty} \left(A_{n,1} \frac{H_n(k_{\text{ext}} r_1)}{H_n'(k_{\text{ext}} a)} - (-1)^n J_n(k_{\text{ext}} r_1) \sum_{m=-\infty}^{\infty} A_{m,1} \frac{H_{m+n}\,(2k_{\text{ext}} d)}{H_m'(k_{\text{ext}} a)} \right) e^{\text{i}n\theta_1}. \tag{7}$$

2.3 Vibro-acoustic response of the cylindrical shell

The shell radial displacement, the acoustic pressure of the interior cavity and the acoustic pressure at any field point in the exterior domain are derived in what follows. The shell model is based on Donnell–Mushtari theory with a Flügge–Byrne–Lur'ye modifying operator [31]. The simplified Flügge equation of motion for the radial displacement of a thin cylindrical shell is given by

$$\frac{1}{\gamma}\left(-\frac{\frac{d^2}{d\theta^2}}{\frac{d^2}{d\theta^2}+a^2k_l^2}+\beta^2\frac{d^4}{d\theta^4}+2\frac{d^2}{d\theta^2}+1+\beta^2-a^2k_l^2\right)w(\theta)=p_{\text{int}}(a,\theta)-p_{\text{ext}}(a,\theta)-f(\theta), \tag{8}$$

where $\gamma=a^2\frac{(1-\nu^2)}{Eh}$, $\beta=\frac{h}{\sqrt{12}a}$ is the dimensionless shell thickness parameter and $k_l=\omega\sqrt{\frac{\rho_s(1-\nu^2)}{E}}$ is the wavenumber for longitudinal waves in the cylindrical shell. The right-hand side of Eq. (8) corresponds to the summation of the various external loads acting on the shell surface comprising the radial line force and the exterior and interior pressure fields.

The same kinematic relationship at the surface of the shell applies to both the interior and exterior fields and is given by

$$\frac{\partial p_{\text{int}}}{\partial r}(a,\theta)=\omega^2\rho_{\text{int}}w(\theta), \tag{9}$$

$$\frac{\partial p_{\text{ext}}}{\partial r}(a,\theta)=\omega^2\rho_{\text{ext}}w(\theta), \tag{10}$$

Employing a Fourier series decomposition, the radial displacement of the shell as well as the interior and exterior acoustic pressures are expressed as follows

$$w(\theta)=\sum_{n=-\infty}^{\infty}w_n e^{\text{i}n\theta}, \tag{11}$$

$$p_{\text{int}}(r,\theta)=\sum_{n=-\infty}^{\infty}P_{n,\text{int}}(r)e^{\text{i}n\theta}, \tag{12}$$

$$p_{\text{ext}}(r,\theta)=\sum_{n=-\infty}^{\infty}P_{n,\text{ext}}(r)e^{\text{i}n\theta}, \tag{13}$$

where w_n are the Fourier coefficients associated with the shell radial displacement, and $P_{n,\text{int}}$, $P_{n,\text{ext}}$ correspond to the Fourier coefficients associated with the interior and exterior pressures, respectively. The radial line force can also be expressed in terms of Fourier coefficients as follows

$$f(\theta)=\sum_{n=-\infty}^{\infty}F_n e^{\text{i}n\theta}. \tag{14}$$

For the line force applied at θ_f as shown in Fig. 1, the Fourier coefficients are given by

$$F_n=\frac{F_f e^{-\text{i}n\theta_f}}{2\pi a}, \tag{15}$$

where F_f is the force amplitude.

The spectral Flügge equation of motion at the shell boundary ($r = a$) is given by

$$\frac{1}{\gamma}\left(-\frac{n^2}{n^2 - a^2k_l^2} + 1 + \beta^2(n^4 - 2n^2 + 1) - a^2k_l^2\right)w_n = P_{n,\text{int}}(a) - P_{n,\text{ext}}(a) - F_n. \tag{16}$$

Solving Eq. (16) for the Fourier coefficients associated with the shell radial displacement yields

$$w_n = \gamma T^{-1}\big(P_{n,\text{int}}(a) - P_{n,\text{ext}}(a) - F_n\big), \tag{17}$$

where $T = -\frac{n^2}{n^2 - a^2k_l^2} + 1 + \beta^2(n^4 - 2n^2 + 1) - a^2k_l^2$.

In what follows, w_n, $P_{n,\text{ext}}$ and $P_{n,\text{int}}$ are expressed in terms of the Fourier coefficient for the exterior acoustic pressure of the submerged cylinder denoted by $A_{n,1}$. Equating Eqs. (7) and (13), the Fourier coefficients for the exterior pressure can be found as

$$P_{n,\text{ext}}(a) = A_{n,1}\frac{H_n(k_{\text{ext}}a)}{H_n'(k_{\text{ext}}a)} - (-1)^n J_n(k_{\text{ext}}a)\sum_{m=-\infty}^{\infty} A_{m,1}\frac{H_{m+n}(2k_{\text{ext}}d)}{H_m'(k_{\text{ext}}a)}, \tag{18}$$

from which the Fourier coefficient of the shell radial displacement can be subsequently found using Eqs. (10) and (11) as follows

$$w_n = \frac{k_{\text{ext}}}{\rho_{\text{ext}}\omega^2}\left(A_{n,1} - (-1)^n J'_n(k_{\text{ext}}a)\sum_{m=-\infty}^{\infty} A_{m,1}\frac{H_{m+n}(2k_{\text{ext}}d)}{H_m'(k_{\text{ext}}a)}\right). \tag{19}$$

Similarly, substituting Eqs. (11) and (12) into Eq. (9) and equating with Eq. (2) yields

$$P_{n,\text{int}}(a) = \frac{\rho_{\text{int}}\omega^2}{k_{\text{int}}}\, w_n \frac{J_n(k_{\text{int}}a)}{J_n'(k_{\text{int}}a)}, \tag{20}$$

Finally, substituting the expressions for Eqs. (15), (19) − (20) into Eq. (17) yields

$$Z_{n,1}A_{n,1} - \sum_{m=-\infty}^{\infty} Z_{(n,m),2}A_{m,1} = -\frac{F_f e^{-in\theta_f}}{2\pi a}, \tag{21}$$

where

$$Z_{n,1} = \frac{(1 - C_{\text{int}})}{\gamma T^{-1}}\frac{k_{\text{ext}}}{\rho_{\text{ext}}\omega^2} + \frac{H_n(k_{\text{ext}}a)}{H_n'(k_{\text{ext}}a)}, \tag{22}$$

$$Z_{(n,m),2} = (-1)^n\frac{H_{m+n}(2k_{\text{ext}}d)}{H_m'(k_{\text{ext}}a)}\left(\frac{(1 - C_{\text{int}})}{\gamma T^{-1}}\frac{k_{\text{ext}}}{\rho_{\text{ext}}\omega^2}J_n'(k_{\text{ext}}a) + J_n(k_{\text{ext}}a)\right). \tag{23}$$

C_{int} accounts for the effect of the internal fluid medium and is given by

$$C_{\text{int}} = \gamma T^{-1}\frac{\rho_{\text{int}}\omega^2}{k_{\text{int}}}\frac{J_n(k_{\text{int}}a)}{J_n'(k_{\text{int}}a)}. \tag{24}$$

Setting the parameter $C_{\text{int}} = 0$ leads to the case of a cylindrical shell with a vacuous interior cavity submerged in a heavy fluid at a finite distance from the free surface. Further, setting $Z_{(n,m),2} = 0$ removes the presence of the free sea surface to yield the case of a cylindrical shell in an unbounded sea.

Solving Eq. (21) yields the solution to $A_{n,1}$. Recalling $p_{fp} = p_1 + p_2$, $A_{n,2} = -A_{-n,1}$, and using Eqs. (3) and (4), where

$$r_2 = \sqrt{(2d - r_1 \sin\theta_1)^2 + (r_1 \cos\theta_1)^2}\,, \tag{25}$$

$$\theta_2 = \frac{3\pi}{2} + \arctan\left(\frac{r_1 \cos\theta_1}{2d - r_1 \sin\theta_1}\right), \tag{26}$$

the acoustic pressure at any field point for the cylindrical shell submerged at a finite depth can be found. Using Eqs. (11) and (19), the shell radial displacement can be determined and further, using Eqs. (12) and (20), the shell interior acoustic pressure is obtained.

3. Results and Discussion

An infinitely long cylindrical shell of thickness $h = 0.01$ m and mid-surface radius $a = 1$ m is modelled. The shell material is steel with properties corresponding to density $\rho_s = 7800$ kg/m^3, Young's modulus $E = 210(1 - 0.02\mathrm{i})$ GPa and Poisson's ratio $\nu = 0.3$. The internal fluid medium is air with density $\rho_{\mathrm{int}} = 1.225$ kg/m^3 and speed of sound $c_{\mathrm{int}} = 343$ m/s. The exterior fluid domain is water with density $\rho_{\mathrm{ext}} = 1000$ kg/m^3 and speed of sound $c_{\mathrm{ext}} = 1500$ m/s. The cylindrical shell is excited by a single radial line force of unity amplitude ($F_f = 1$ N/m) at $\theta_f = \pi/2$.

Table 1 lists the structural and internal acoustic resonances of the cylindrical shell in an unbounded domain for a frequency range up to 200 Hz. In this frequency range, ten structural resonances and two internal acoustic resonances occur. The acoustic resonances within the shell cavity correspond to (p, q) modes, where p is the number of plane diametral nodal surfaces and q is the number of cylindrical nodal surfaces concentric with the cylinder axis [32]. The effect of a heavy external fluid (water) and light fluid (air) on the shell structural and internal acoustic resonances can be observed. The frequency of the structural resonances for the shell in water are significantly lower than the resonant frequencies of the shell in air due to the increased added mass effect from the surrounding fluid. In contrast, the presence of significant fluid loading (water) only slightly reduces the internal acoustic resonances of the shell. Fig. 3 presents the shell radial velocity at $\theta = 3\pi/2$, for two different immersion depths corresponding to $d = 5a$ and $d = 10a$. Results for the cylindrical shell in an unbounded sea are also presented. The peaks correspond to circumferential modes of order n. While Fig. 3 shows that variation in immersion depth has negligible impact on the shell vibrational characteristics, the results were obtained neglecting the influence of external hydrostatic pressure. Previous studies have shown that the structural responses of a point driven infinite cylindrical shell can be strongly affected by hydrostatic pressure [33]. An increase in external hydrostatic pressure may increase the hoop membrane compressive stress of the cylindrical shell and reduce the frequency of the structural resonances [33, 34].

Fig. 4 presents the interior acoustic pressure at $(r, \theta) = (0.5a, 3\pi/2)$. Similar to Fig. 3, the peaks are labelled by their corresponding structural or internal acoustic modal order. Fig. 4 shows that only the structural resonances that occur below the first cavity resonance contribute to the interior acoustic pressure, beyond which the cavity resonances dominate the response. Comparison of Fig. 3 and Fig. 4 reveals that the cavity resonances do not affect the shell vibration, attributed to the fact that the interior fluid is a light fluid.

Fig. 5 presents the exterior acoustic pressure as a function of frequency at a field point location of $(r, \theta) = (5a, 3\pi/2)$ for the two different immersion depths of $d = 5a$ and $d = 10a$, as well as the acoustic pressure in an unbounded domain. Variation in immersion depth is shown to have a strong influence on the amplitude of the external pressure, whereby the acoustic pressure associated with a finite depth oscillates about the pressure for the unbounded case. Fig. 6 extends the results in Fig. 5 to examine the effect of very large immersion depths on the exterior acoustic pressure. Similar to Fig. 5, Fig. 6 shows that only the lowest order structural and acoustic resonances play a significant role on the amplitude of the exterior acoustic pressure. It is clearly observed that increasing the immersion depth results in a decrease in both the period and amplitude of the oscillating pressure.

The oscillations in the acoustic pressure are attributed to the alternating constructive and destructive interferences caused by the reflection of the free surface, as described by Li et al. [24]. With increasing depth, the acoustic field for the bounded case converges towards the acoustic pressure of the unbounded case, as previously reported [26].

Table 1. Structural and internal acoustic resonances of a cylindrical shell in water and in air for a frequency range up to 200 Hz. Cylindrical shell is in an unbounded domain.

Type	Modal order	Frequency (Hz) (Shell in water)	Frequency (Hz) (Shell in air)
Structural	1	0	0
Structural	2	2.71	6.66
Structural	3	8.61	18.88
Structural	4	18.14	36.24
Structural	5	31.58	58.64
Structural	6	49.15	86.06
Structural	7	70.98	118.50
Structural	8	97.23	155.91
Acoustic	(1,0)	100.55	100.84
Structural	9	127.97	198.38
Structural	10	163.26	245.78
Acoustic	(2,0)	166.79	167.12

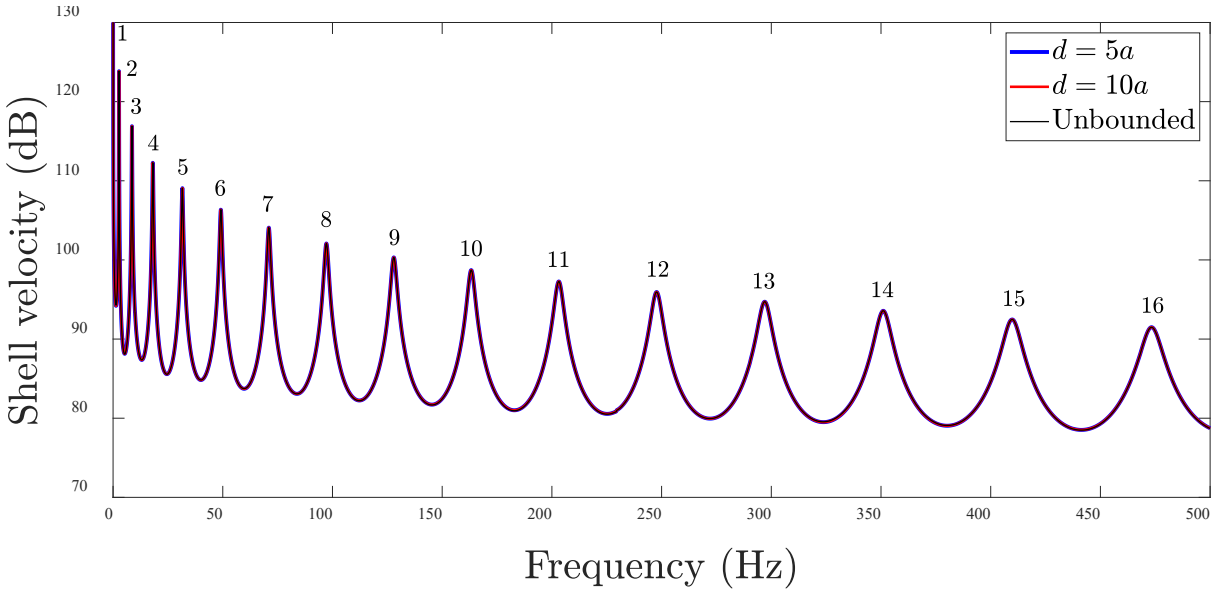

Fig. 3. Shell velocity at $\theta = 3\pi/2$ (dB ref. 1 nm/s). The structural resonances are labelled by their order.

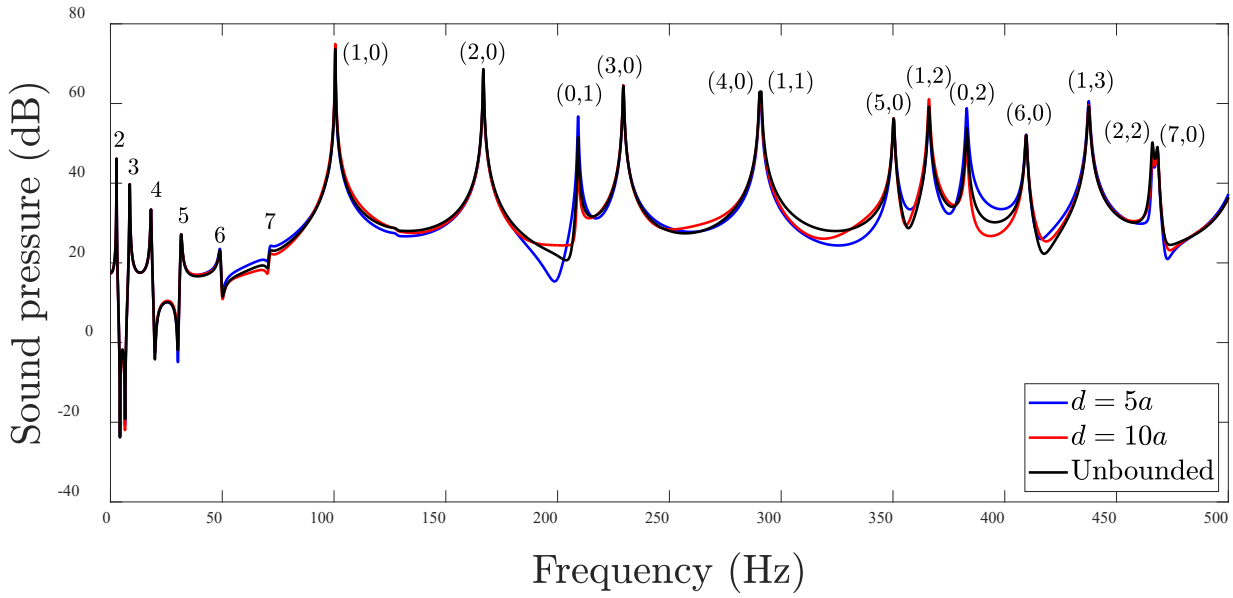

Fig. 4. Internal sound pressure level at $r = 0.5a$ and $\theta = 3\pi/2$ (dB ref. 20 μPa) . The structural and internal acoustic resonances are labelled by their order.

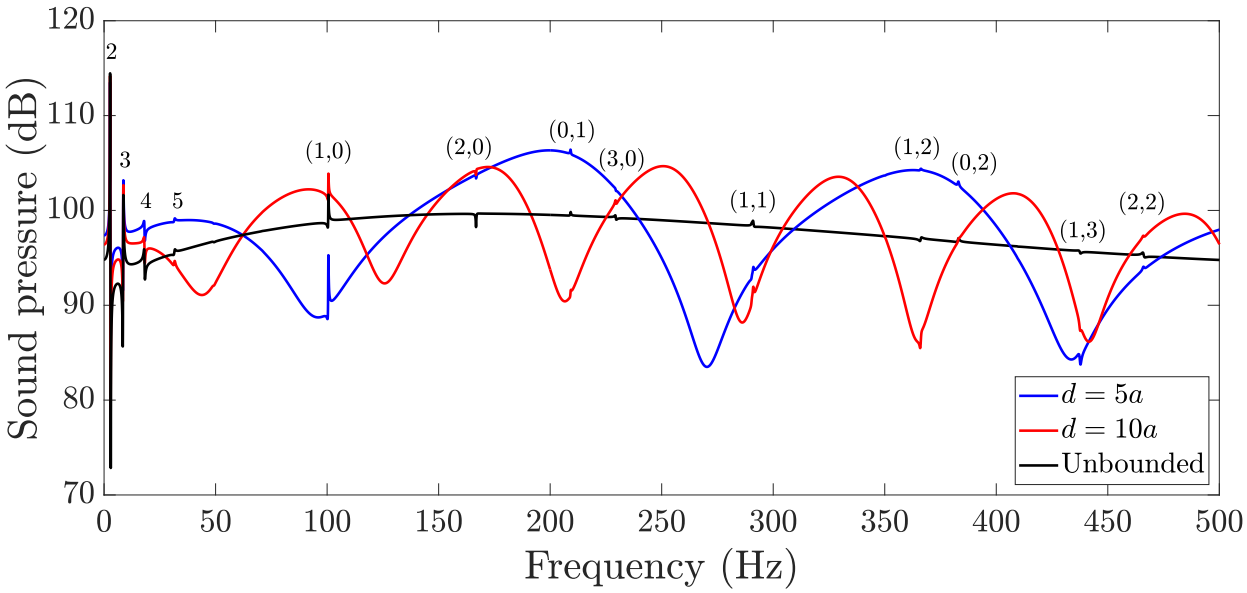

Fig. 5. External sound pressure level at $r = 5a$ and $\theta = 3\pi/2$ (dB ref. 1 μPa). The structural and internal acoustic resonances are labelled by their order.

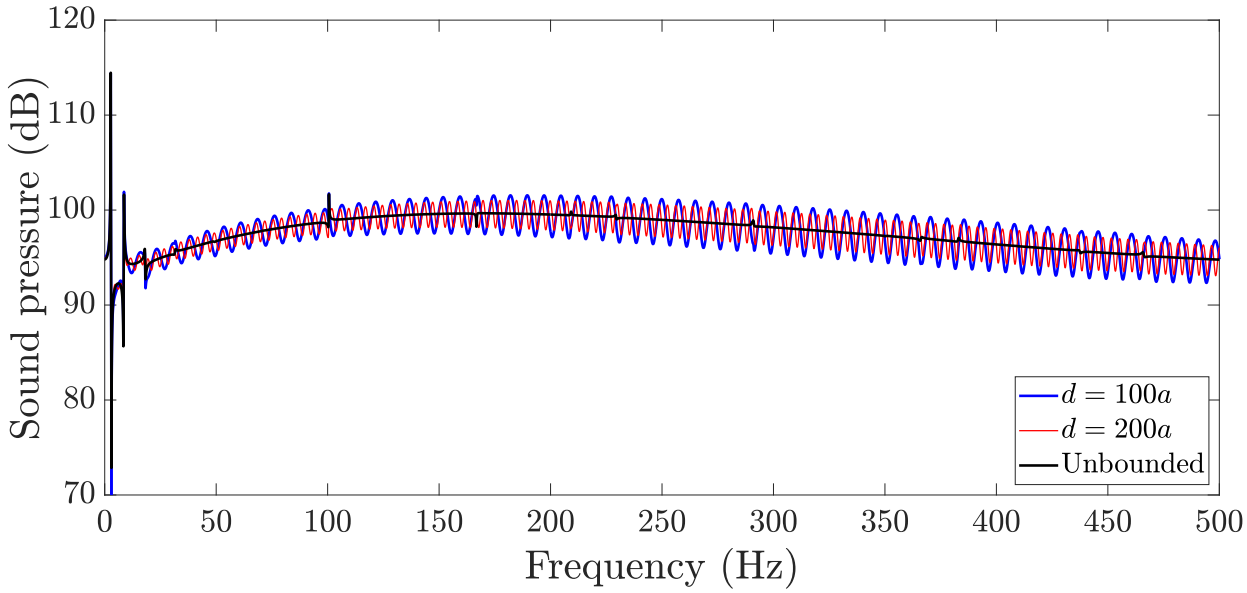

Fig. 6. External sound pressure level at $r = 5a$ and $\theta = 3\pi/2$ (dB ref. 1 μPa).

Fig. 7 presents the exterior acoustic pressure predicted using the current model for the cylindrical shell submerged at $d = 5a$ and $d = 10\,a$. Results are compared with those from a 'mirror effect' model, corresponding to a model in which the exterior acoustic pressure for the submerged cylinder was calculated taking into account reflections from the free surface but neglecting any effect of the free surface on the shell vibrational response. This was achieved by setting $Z_{(n,m),2} = 0$ in Eq. (21) to yield the Fourier coefficients for the exterior acoustic pressure denoted by $A_{n,1}$, which are subsequently used with Eqs. (25) and (26) to calculate the total acoustic pressure for the submerged cylinder. Whilst there is good agreement between the two models at low frequencies, it is apparent that discrepancies increase with increasing frequency. This is attributed to the fact that the acoustic wavelength decreases with increasing frequency, leading to greater interaction of reflected waves with the shell vibrations which are subsequently dissipated by the shell.

Contour plots of the acoustic pressure fields for the two immersion depths corresponding to $d = 5a$ and $d = 10a$ are presented at two low order structural resonances (Fig. 8) and at the two shell cavity resonances (Fig. 9). Results are also compared to contour plots of the acoustic pressure for the cylindrical shell in an unbounded fluid. In Fig. 8, the deformation of the shell at its 2nd and 3rd structural resonances shows the presence of two and three plane diametral nodal surfaces, respectively. Similarly, in Fig. 8, pressure contours of the (1,0) and (2,0) internal acoustic resonances show one or two plane diametral nodal surfaces and zero cylindrical nodal surfaces. Close to the free surface ($d = 5a$), reflection at the boundary can be observed. It will be subsequently shown that the mirror effect depends on the non-dimensional ratio $2d/\lambda$ where λ is the acoustic wavelength associated with the exterior acoustic domain.

Whilst reciprocity between the distance to the free surface and the acoustic wavelength occurs for simple acoustic sources, this result no longer occurs for a submerged elastic shell. Moreover, it was shown in Fig. 7 that the vibro-acoustic response of the shell is influenced by the interaction between reflections from the free surface and the shell vibrational response. The influence of a free sea surface is now explored by examining the individual contributions of the Fourier coefficients associated with the shell radial displacement and structurally radiated pressure on the structural and acoustic responses of the submerged shell. Fig 10 presents the lowest order Fourier coefficients of the shell radial displacement w_n, as well as the summation of all Fourier coefficients that cut on in the frequency range up to 500 Hz, in an unbounded sea (Fig 10 (a)) and immersed near a free surface at $d = 10a$ (Fig 10 (b)) and $d = 30a$ (Fig 10 (c)). For $n \geq 1$, the contributions of successive Fourier coefficients to the total response can be clearly observed. Beyond the peak frequency for each Fourier coefficient, all Fourier coefficients asymptote to a decreasing value with similar contribution to the total response. Very small peaks at frequencies corresponding to the internal acoustic resonances can also be observed in both the unbounded and bounded cases, associated with the acoustic-structure interaction between the shell and its interior cavity. The presence of an acoustic resonance for a given number of plane diametral nodal surfaces occurs at the corresponding modal order of the structural resonance. That is, at the Fourier coefficient of the shell radial displacement associated with $n = 1$, a small peak corresponding to the internal acoustic resonance of (1,0) at around 100 Hz can be observed. Similarly, at the structural Fourier coefficient for $n = 2$, the internal acoustic resonance of (2,0) at around 167 Hz can be observed. For the cylindrical shells immersed at a finite depth, ripples in the Fourier coefficients with increasing frequency can be observed, attributed to reflections from the free surface. However, these ripples only occur for the lowest circumferential orders and do not have any significant effect on the shell vibratory response.

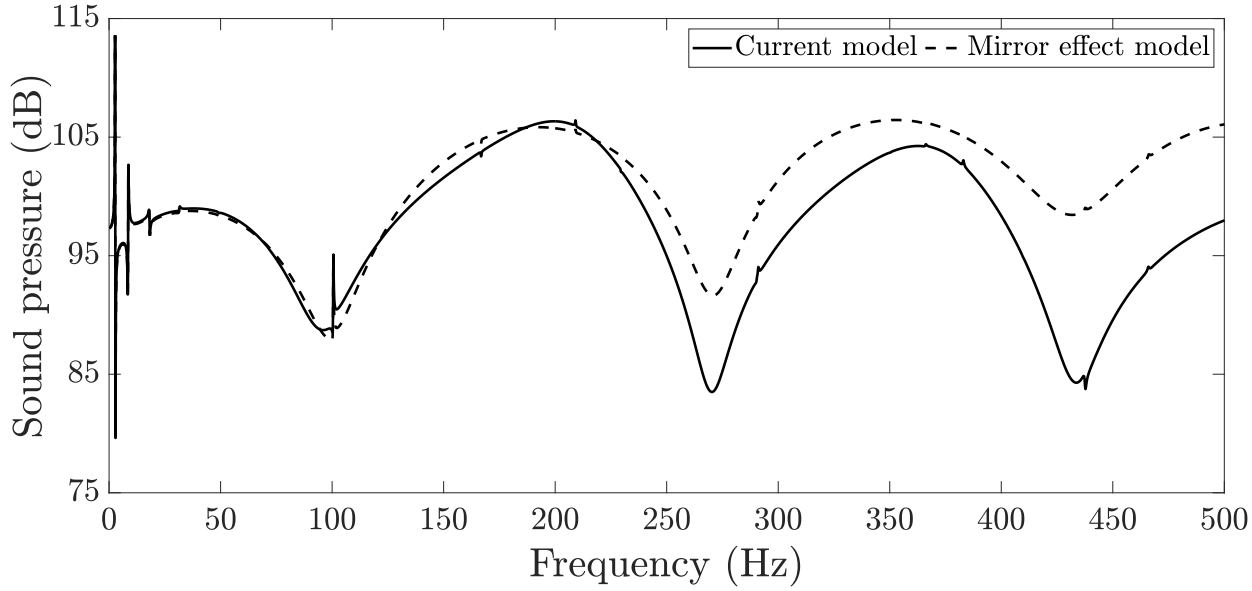

(a)

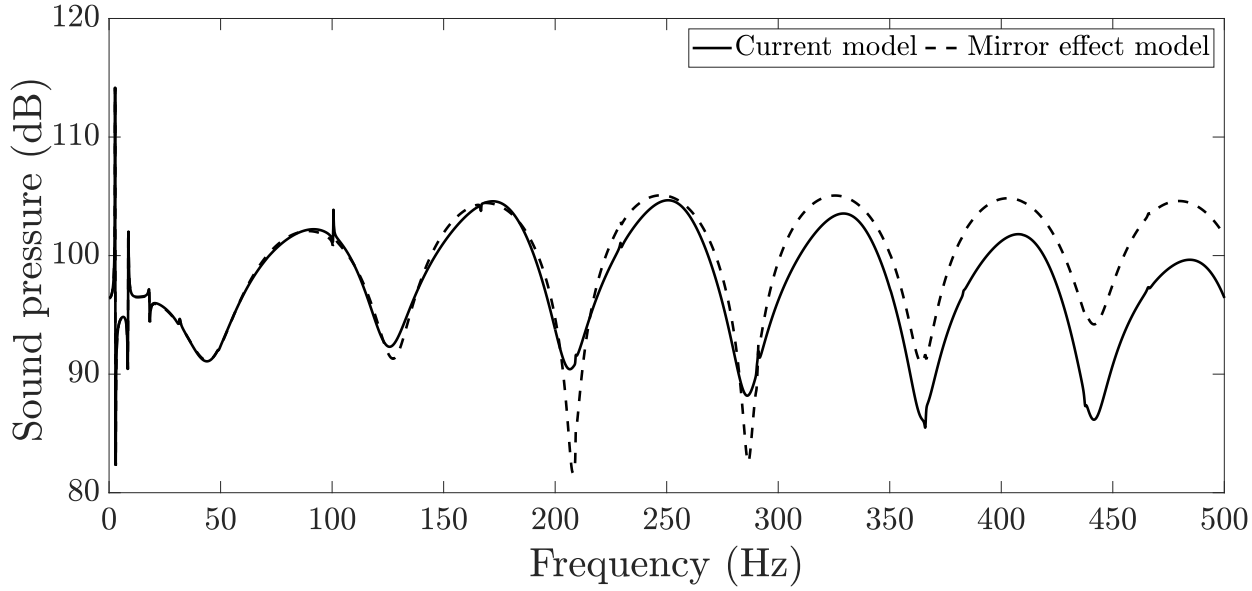

(b)

Fig. 7. External sound pressure level at $r = 5a$ and $\theta = 3\pi/2$ (dB ref. 1 μPa) for the cylindrical shell submerged at (a) $d = 5a$ and (b) $d = 10a$. The mirror effect model is denoted by the dashed line.

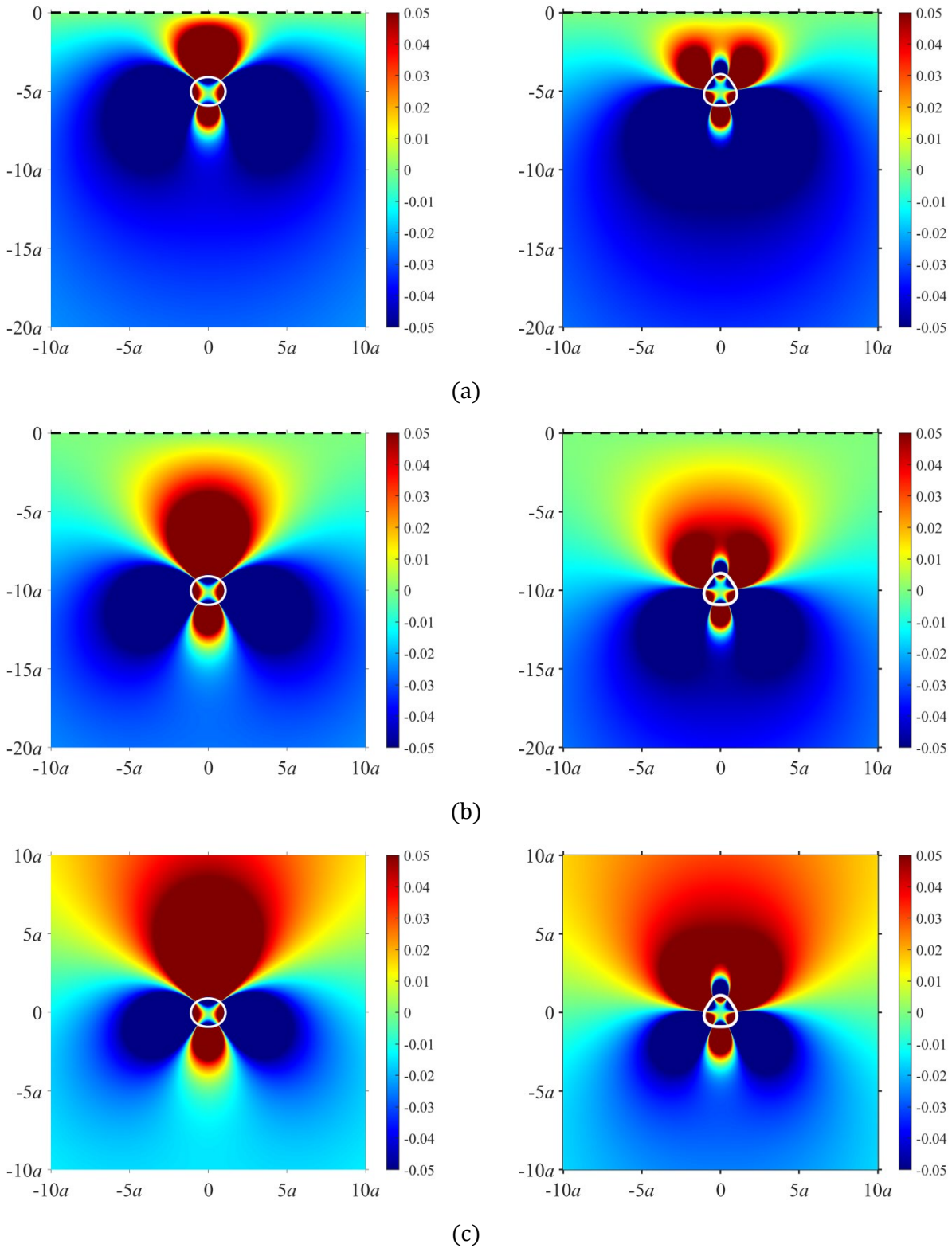

Fig. 8. Pressure contour and shell displacement for immersion depth of (a) $d = 5a$, (b) $d = 10a$, and (c) in an unbounded domain at the second structural resonance of 2.7 Hz (left) and the third structural resonance of 8.6 Hz (right). The free surface is represented by the black dashed line at $d = 0$ in (a) and (b). The shell displacement is scaled for clearer visualisation of the deformation. The internal pressure field is multiplied by 10^2 for greater visual contrast.

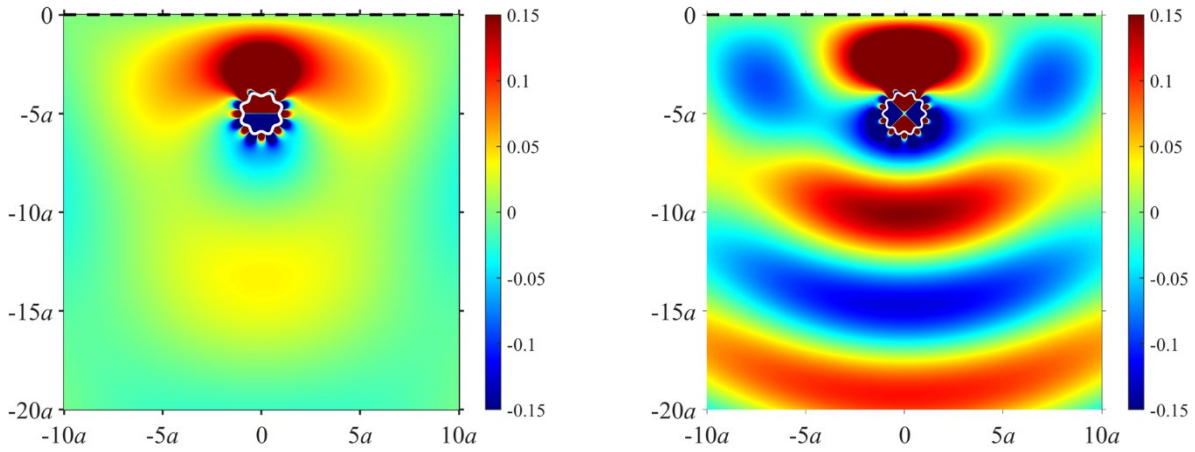

(a)

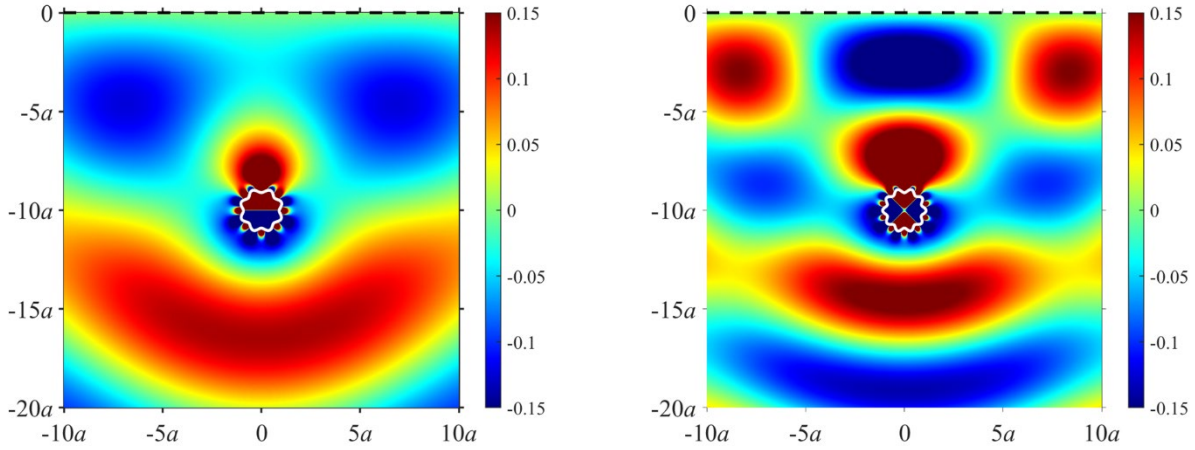

(b)

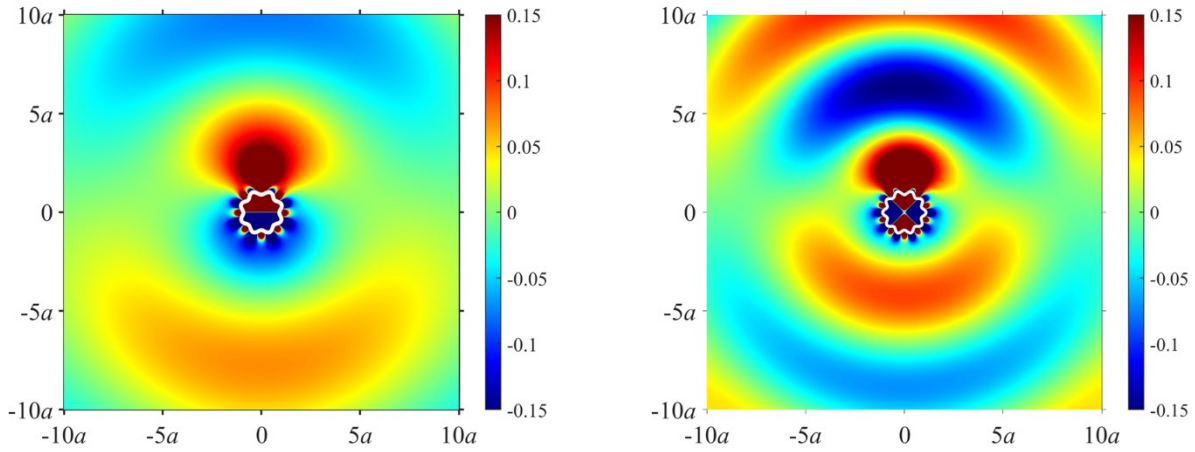

(c)

Fig. 9. Pressure contour and shell displacement for immersion depth of (a) $d = 5a$, (b) $d = 10a$, and (c) in an unbounded domain at the $(p, q) = (1,0)$ internal acoustic resonance of 100.6 Hz (left) and the $(p, q) = (2,0)$ internal acoustic resonance of 166.9 Hz (right). The free surface is represented by the black dashed line at $d = 0$ in (a) and (b). The shell displacement is scaled for clearer visualisation of the deformation. The internal pressure field is multiplied by 10^2 for greater visual contrast.

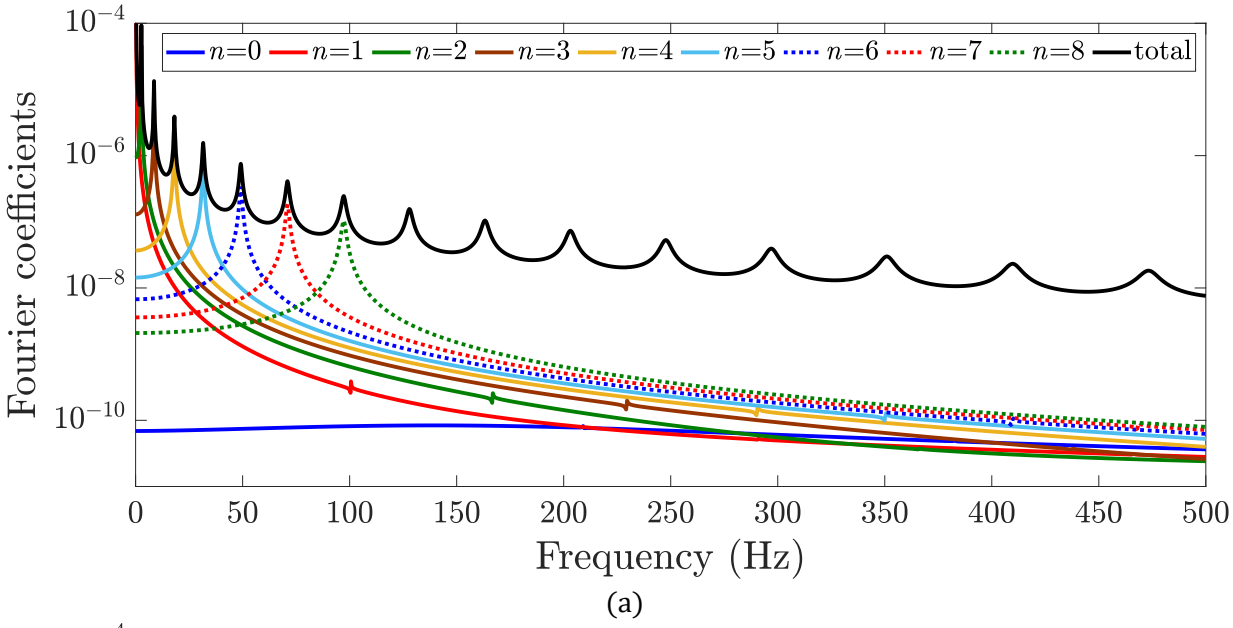

(a)

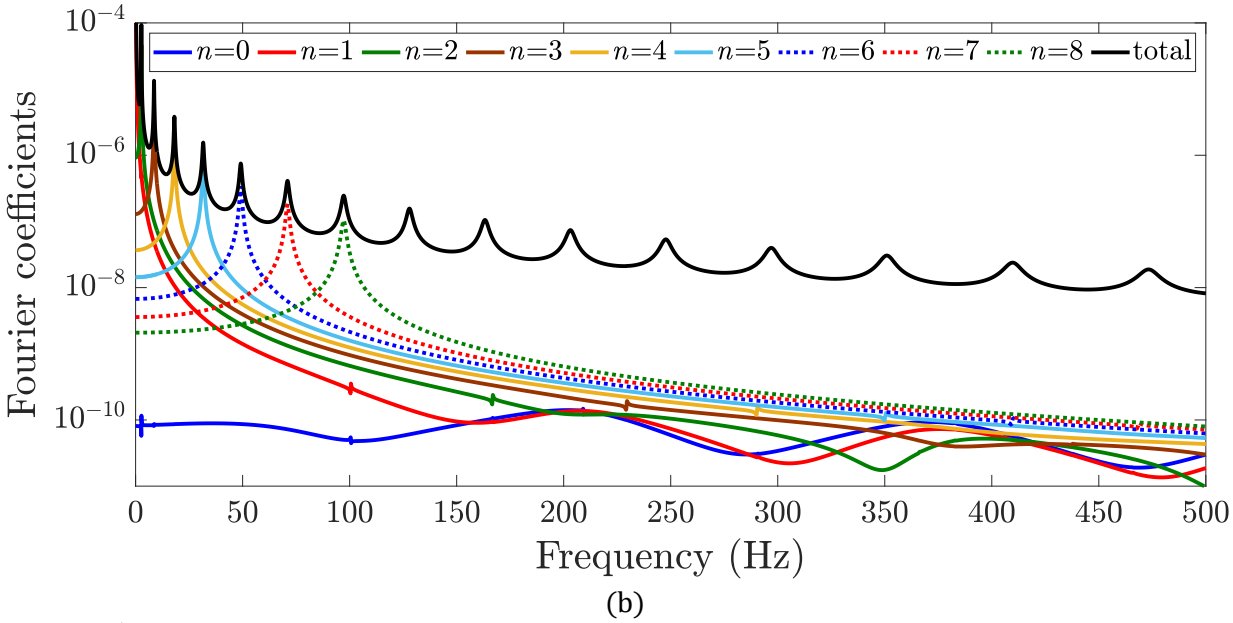

(b)

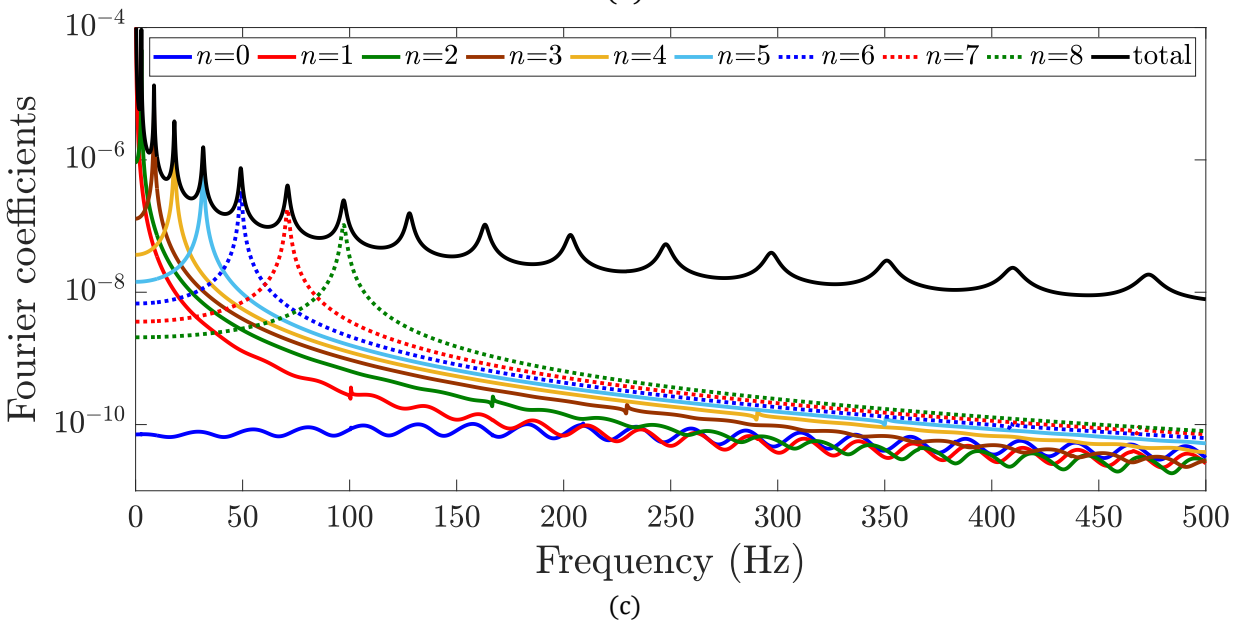

(c)

Fig 10. Summation of the Fourier coefficients for the shell radial displacement w_n as well as the individual contributions from the lowest order modes for (a) the cylindrical shell in an unbounded sea, and for the cylindrical shell immersed at a finite depth of (b) $d = 10a$ and (c) $d = 30a$.

Fig. 11 presents the individual normalised Fourier coefficients for the external pressure, $A_n/H'_n(k_{\text{ext}}a)$, as well as the summation of all normalised Fourier coefficients that cut on in the frequency range up to 500 Hz, in an unbounded sea (Fig. 11 (a)), and immersed near a free surface at $d = 10$a (Fig. 11 (b)) and $d = 30$a (Fig. 11 (c)). Similar to the Fourier coefficients for the shell displacement, successive Fourier coefficients for the acoustic pressure cut on with increasing frequency. At low frequencies, the lowest order Fourier coefficients dominate the total acoustic response. As a result, the ripples associated with the low circumferential orders have a significant influence on the radiated pressure. As the frequency increases, the contributions from all Fourier coefficients increase asymptotically and converge towards a similar value. The presence of a small peak associated with the internal cavity resonances can also be observed at the corresponding order of the Fourier coefficient. Ripples in the acoustic pressure associated with the presence of a free surface can be observed. The free surface has a stronger influence on the total acoustic pressure (Fig. 11 (b) and Fig. 11 (c)) compared to the total shell response (Fig 10 (b) and Fig 10 (c)). An increase in the immersion depth also results in a decrease in the period of the oscillating pressure, as discussed previously in Fig. 6.

To further explore the phenomena associated with the presence of the ripples observed in Fig. 10 and Fig. 11, Fig. 12 presents the ratio of the Fourier coefficients for the cylindrical shell immersed near a free surface at $d = 10a$ (Fig. 12 (a)) and $d = 30a$ (Fig. 12 (b)) to those for the cylinder in an unbounded sea, as a function of the non-dimensionalised frequency $k_{\text{ext}}a$. Similar to the results observed in Figs. 10 and 11, successive modal orders cut on with increasing frequency. The period of oscillations for each modal order is very similar and corresponds to a non-dimensional ratio of around $0.5d/\lambda$. However, the amplitude of the modulation decreases with increasing immersion depth. Fig. 11 shows that the presence of a free sea surface has a strong influence on modal orders for $k_{\text{ext}}a \geq n$. Coupling between the lowest order shell circumferential orders and the internal acoustic resonances of the same modal order can also be observed.

The influence of the immersion depth is now studied at a discrete excitation frequency. Fig. 13 (a) presents the ratio of the external pressure of the cylindrical shell immersed at depth d to the external pressure for the cylindrical shell in an unbounded sea, as a function of the non-dimensional frequency d/λ at 500 Hz ($\sim 2.1\ k_{\text{ext}}a$). The period of the oscillations is $0.5d/\lambda$ and is attributed to the alternating constructive and destructive interferences caused by the reflection of the free surface, as described previously by Li et al. [24]. The amplitude decays by $\sqrt{2/d}$ with increasing depth, attributed to cylindrical spreading of sound waves in the radial direction. Both the current model and mirror effect model display the same periodic oscillations but differ in amplitude, attributed to the fact that the mirror effect model does not consider the interaction between the reflected waves and shell vibration and hence the energy dissipated by the shell. Fig. 13 (b) presents the ratio of Fourier coefficients of the submerged cylindrical shell to the Fourier coefficients for the cylindrical shell submerged in an unbounded sea, for the lowest order shell circumferential orders at a frequency of 500 Hz. Similar to the results in Fig. 13 (a), the periodicity of $0.5d/\lambda$ at each circumferential order can be observed and the ratio for each Fourier coefficient decays by $\sqrt{2/d}$ with increasing depth. As discussed previously in Fig. 12, the lowest order circumferential orders have the highest amplitude at this frequency, followed by the contributions from subsequent circumferential orders. These results highlight the combined influence of the lowest order shell circumferential modes and immersion depth to the vibro-acoustic response of a submerged cylindrical shell.

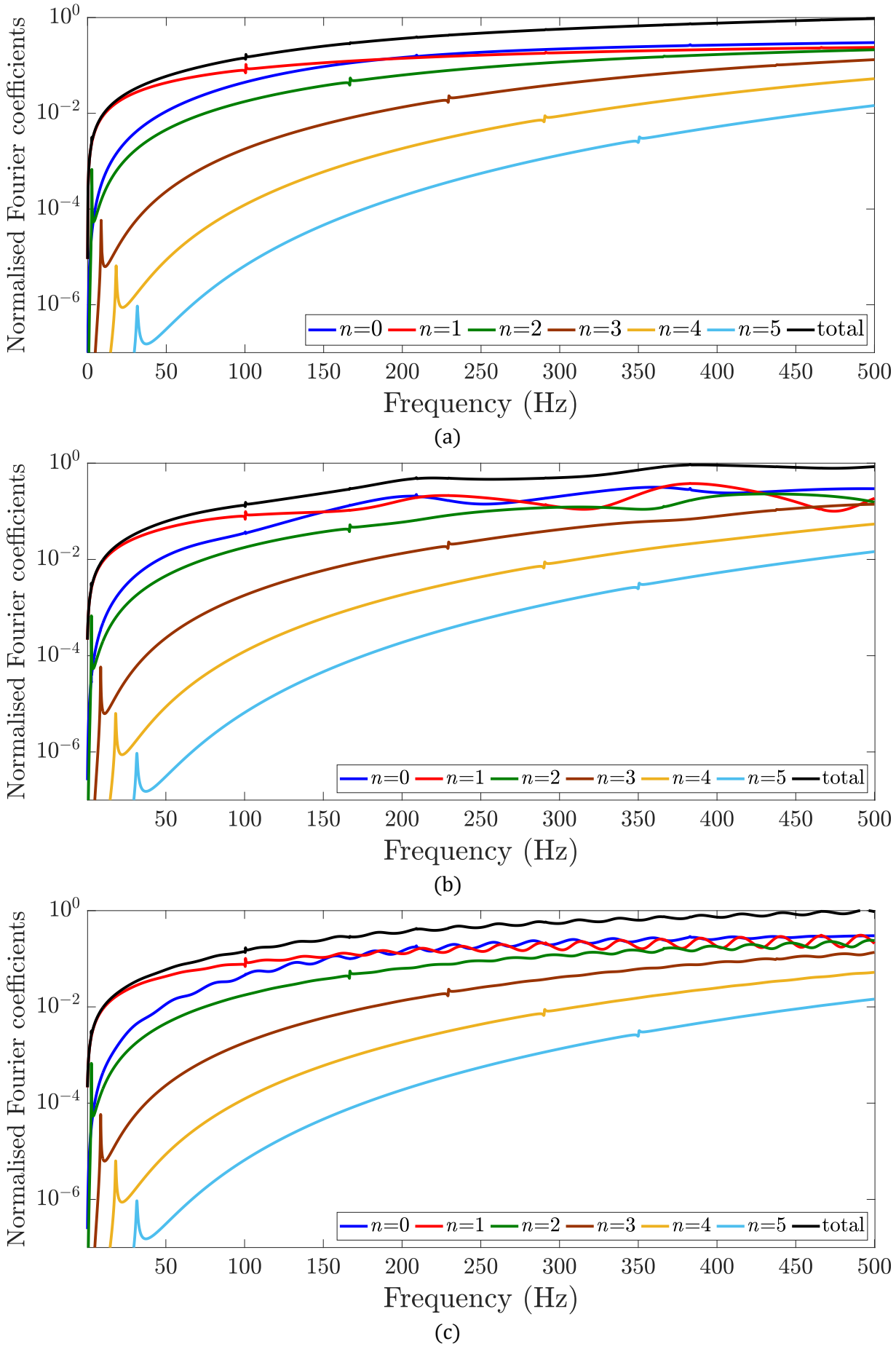

Fig. 11. Summation of the normalised Fourier coefficients $A_n/H'_n(ka)$ for the external pressure as well as the individual contributions from the lowest order modes for (a) the cylindrical shell in an unbounded sea, and for the cylindrical shell immersed at a finite depth of (b) $d = 10a$ and (c) $d = 30a$.

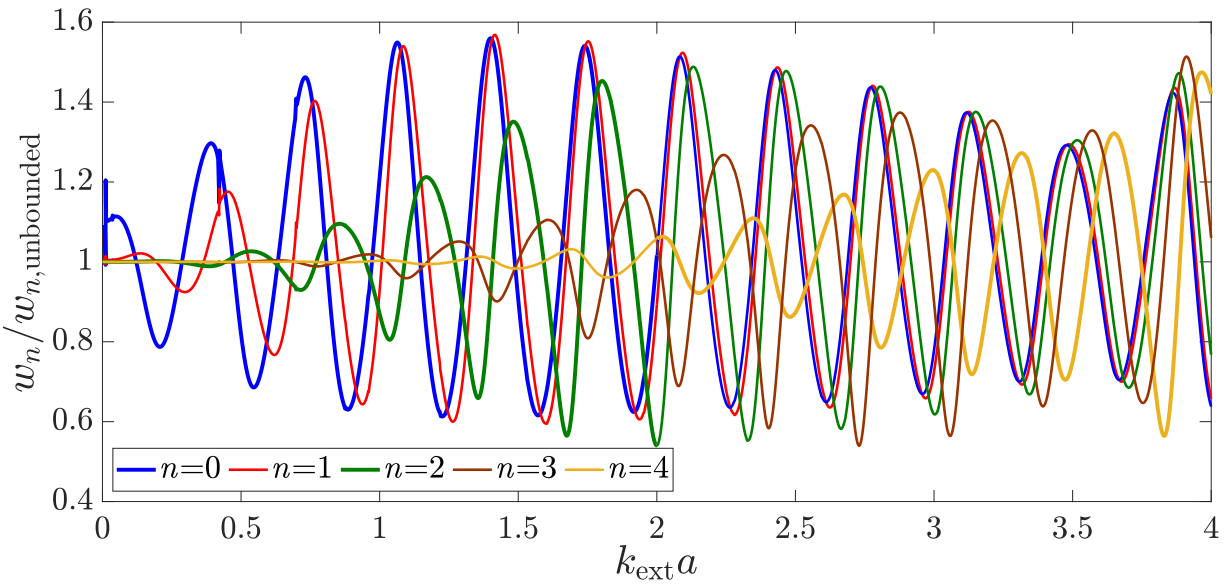

(a)

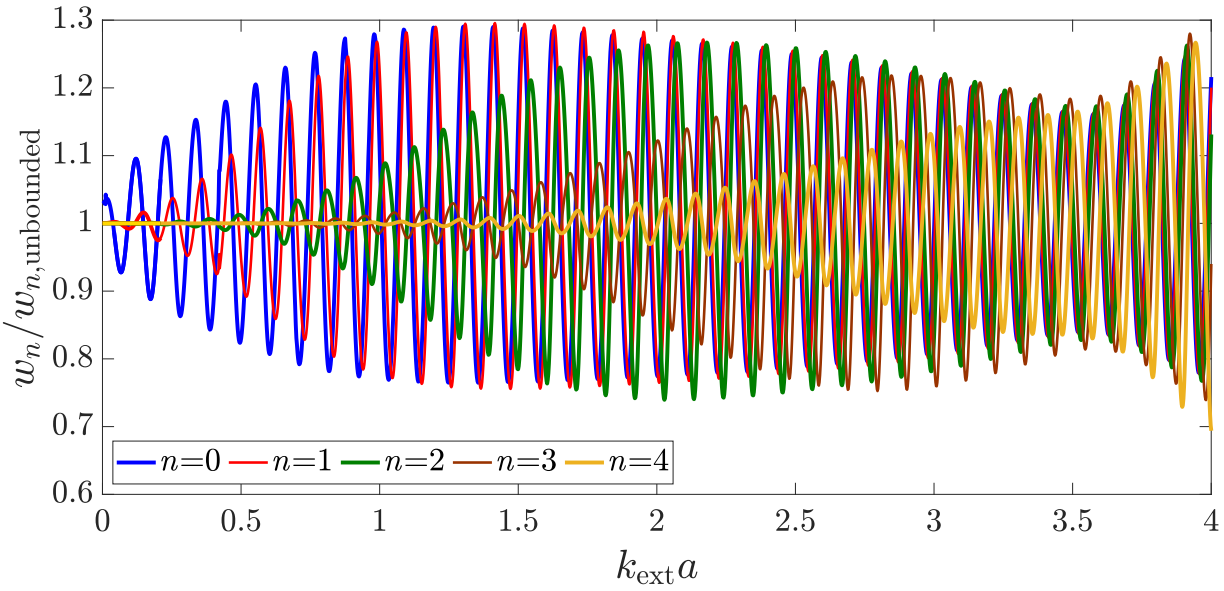

(b)

Fig. 12. Ratio of the Fourier coefficients for the cylindrical shell submerged at (a) $d = 10a$ and (b) $d = 30a$ to the Fourier coefficients for a cylindrical shell in an unbounded sea, as a function of the non-dimensionalised frequency $k_{ext}a$ (corresponding to a frequency range up to 955 Hz).

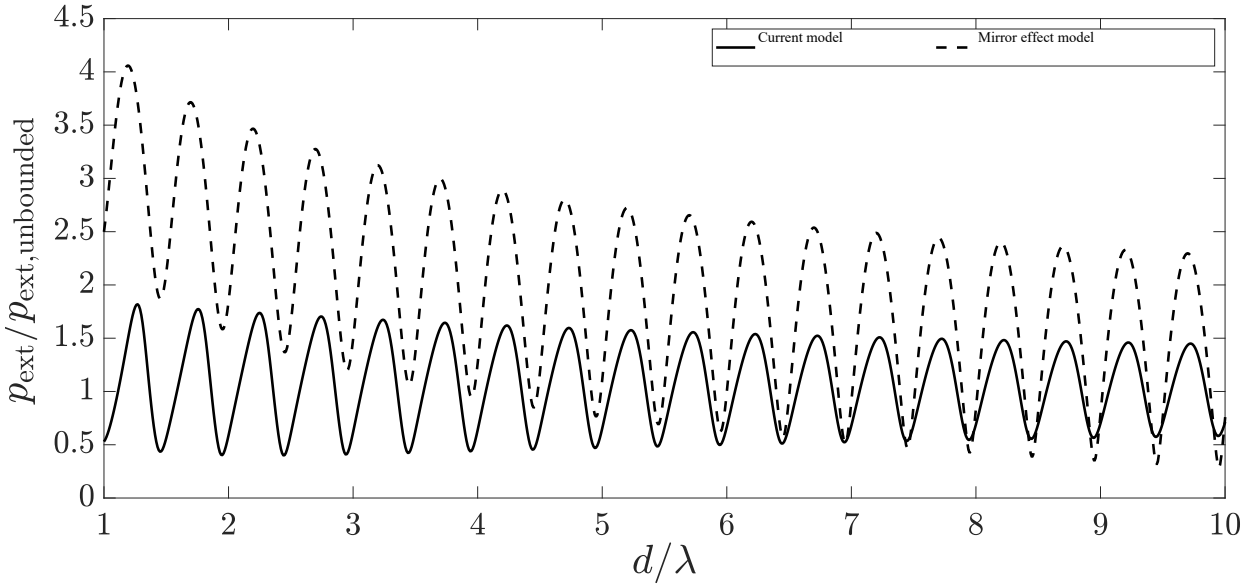

(a)

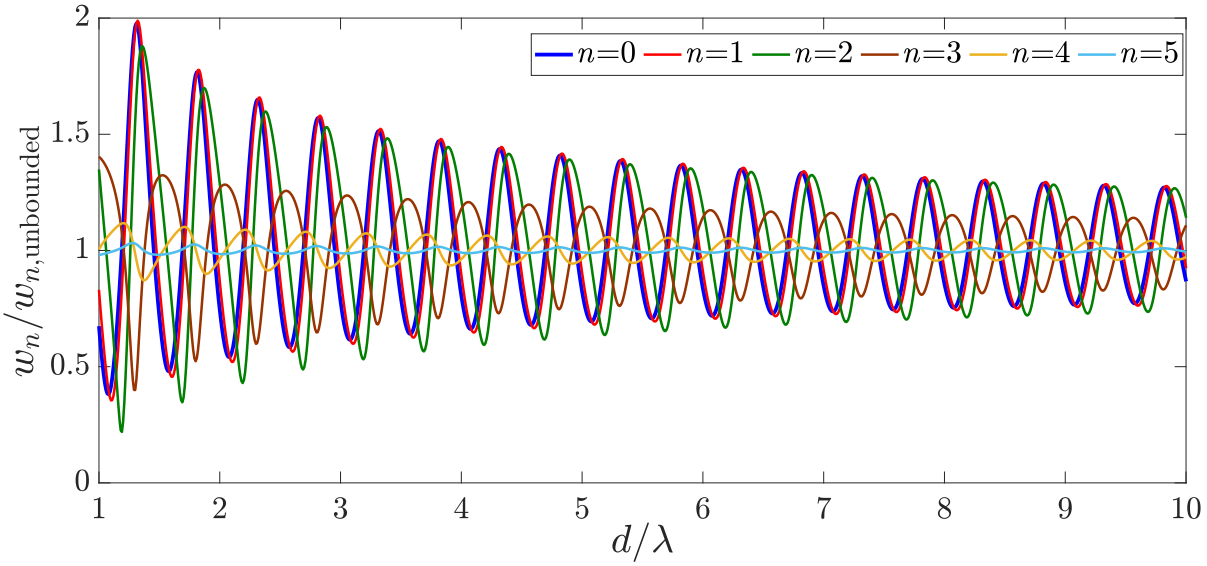

(b)

Fig. 13. (a) Ratio of the external pressure of the submerged cylindrical shell to the external pressure for a cylindrical shell in an unbounded sea at $(r, \theta) = (5a, 3\pi/2)$ and 500 Hz, and (b) ratio of the Fourier coefficients of the submerged cylindrical shell to the Fourier coefficients for a cylindrical shell in an unbounded sea at 500 Hz, as a function of the non-dimensionalised ratio d/λ.

4. Conclusions

A theoretical model of an infinite cylindrical shell submerged at a finite distance from the free sea surface has been presented. The elastic shell is fully coupled with the interior and exterior acoustic fluids. Analytical expressions for the shell displacement, internal acoustic pressure and acoustic pressure in the exterior domain near a free sea surface are derived. In contrast to previous work that derives the far-field pressure using the method of stationary phase, the current model predicts the acoustic pressure in both the near field and far field of the cylindrical shell. However, the analytical formulation only considers a linear vibro-acoustic problem neglecting the influence of external hydrostatic pressure. Results reveal insight into the physical mechanisms of the submerged hull at a finite distance from a free surface. The combined effect of the free sea surface and the individual shell circumferential modes on the structural and acoustic responses of the shell were examined in detail. Variation in immersion depth was observed to have a strong influence on the amplitude of the external pressure. The vibro-acoustic response of the shell was also shown to be influenced by the effect of reflections in proximity to the free surface and the lowest order shell circumferential modes.

5. References

[1] M.C. Junger, D. Feit, Sound, Structures, and their Interaction, 2nd ed, MIT Press, Cambridge, MA, 1986.

[2] B.E. Sandman, Fluid-loading influence coefficients for a finite cylindrical shell, J. Acoust. Soc. Am. 60 (1976) 1256–1264. https://doi.org/10.1121/1.381238.

[3] G.C. Everstine, Prediction of low frequency vibrational frequencies of submerged structures, J. Vib. Acoust. 113 (1991) 187–191. https://doi.org/10.1115/1.2930168.

[4] J.F.M. Scott, The free modes of propagation of an infinite fluid-loaded thin cylindrical shell, J. Sound Vib. 125 (1988) 241–280. https://doi.org/10.1016/0022-460X(88)90282-9.

[5] D.M. Photiadis, The propagation of axisymmetric waves on a fluid-loaded cylindrical shell, J. Acoust. Soc. Am. 88 (1990) 239–250. https://doi.org/10.1121/1.400348.

[6] P.R. Stepanishen, Modal coupling in the vibration of fluid-loaded cylindrical shells, J. Acoust. Soc. Am. 71 (1982) 813–823. https://doi.org/10.1121/1.387607.

[7] L.B. Felsen, J.M. Ho, I.T. Lu, Three-dimensional Green's function for fluid-loaded thin elastic cylindrical shell: Formulation and solution, J. Acoust. Soc. Am. 87 (1990) 543–553. https://doi.org/10.1121/1.398925.

[8] G.C. Everstine, F.M. Henderson, Coupled finite element/boundary element approach for fluid–structure interaction, J. Acoust. Soc. Am. 87 (1990) 1938–1947. https://doi.org/10.1121/1.399320.

[9] J. Mackerle, Fluid–structure interaction problems, finite element and boundary element approaches A bibliography (1995–1998), Finite Elem. Anal. Des. 31 (1999) 231–240. https://doi.org/10.1016/S0168-874X(98)00065-1.

[10] R.A. Jeans, L.C. Mathews, Solution of fluid-structure interaction problems using a coupled finite element and variational boundary element technique, J. Acoust. Soc. Am. 88 (1990) 2459–2466. https://doi.org/10.1121/1.400086.

[11] D. Brunner, M. Junge, L. Gaul, A comparison of FE-BE coupling schemes for large-scale problems with fluid-structure interaction, Int. J. Numer. Methods Eng. 77 (2009) 664–688. https://doi.org/10.1002/nme.2412.

[12] H. Peters, N. Kessissoglou, S. Marburg, Modal decomposition of exterior acoustic-structure interaction problems with model order reduction, J. Acoust. Soc. Am. 135 (2014) 2706–2717. https://doi.org/10.1121/1.4869086.

[13] P. Salaün, Effect of a free surface on the far-field pressure radiated by a point-excited cylindrical shell, J. Acoust. Soc. Am. 90 (1991) 2173–2181. https://doi.org/10.1121/1.402373.

[14] I. Rudnick, The propagation of an acoustic wave along a boundary, J. Acoust. Soc. Am. 19 (1947) 348–356. https://doi.org/10.1121/1.1916490.

[15] U. Ingard, G.L. Lamb, Effect of a reflecting plane on the power output of sound sources, J. Acoust. Soc. Am. 29 (1957) 743–744. https://doi.org/10.1121/1.1909034.

[16] D.I. Paul, Acoustical radiation from a point source in the presence of two media, J. Acoust. Soc. Am. 29 (1957) 1102–1109. https://doi.org/10.1121/1.1908712.

[17] E.G. McLeroy, Complex image theory of low-frequency sound propagation in shallow water, J. Acoust. Soc. Am. 33 (1961) 1120–1126. https://doi.org/10.1121/1.1908915.

[18] E.J. Skudrzyk, The Foundations of Acoustics, Springer-Verlag, New York, 1971.

[19] J.C. Bertrand, J.W. Young, Multiple scattering between a cylinder and a plane, J. Acoust. Soc. Am. 60 (1976) 1265–1269. https://doi.org/10.1121/1.381239.

[20] Z. Ye, C. You-Yu, Acoustic scattering by a cylinder near a pressure release surface, ArXiv.Org. (2001). http://search.proquest.com/docview/2091888792/?pq-origsite=primo (accessed June 9, 2020).

[21] W.K. Lui, K.M. Li, The scattering of sound by a long cylinder above an impedance boundary, J. Acoust. Soc. Am. 127 (2010) 664–674. https://doi.org/10.1121/1.3273891.

[22] S.M. Hasheminejad, M. Azarpeyvand, Modal vibrations of a cylindrical radiator over an impedance plane, J. Sound Vib. 278 (2004) 461–477. https://doi.org/10.1016/j.jsv.2003.10.039.

[23] A. Ergin, P. Temarel, Free vibration of a partially liquid-filled and submerged, horizontal cylindrical shell, J. Sound Vib. 254 (2002) 951–965. https://doi.org/10.1006/jsvi.2001.4139.

[24] T.Y. Li, Y.Y. Miao, W.B. Ye, X. Zhu, X.M. Zhu, Far-field sound radiation of a submerged cylindrical shell at finite depth from the free surface, J. Acoust. Soc. Am. 136 (2014) 1054–1064. https://doi.org/10.1121/1.4890638.

[25] W. Guo, T. Li, X. Zhu, Far-field acoustic radiation and vibration of a submerged finite cylindrical shell below the free surface based on energy functional variation principle and stationary phase method, Noise Control Eng. J. 65 (2017) 565–576. https://doi.org/10.3397/1/376570.

[26] W. Guo, T. Li, X. Zhu, Y. Miao, G. Zhang, Vibration and acoustic radiation of a finite cylindrical shell submerged at finite depth from the free surface, J. Sound Vib. 393 (2017) 338–352. https://doi.org/10.1016/j.jsv.2017.01.003.

[27] P.A. Martin, ed., Addition theorems in two dimensions, in: Mult. Scatt. Interact. Time-Harmon. Waves N Obstacles, Cambridge University Press, Cambridge, 2006: pp. 29–61. https://doi.org/10.1017/CBO9780511735110.003.

[28] D. Ross, Mechanics of Underwater Noise, Pergamon Press, New York, 1976.

[29] M. Abramowitz, I.A. Stegun, Handbook of mathematical functions., Dover, New York, 1965.

[30] W. Meng, L. Wang, Bounds for truncation errors of Graf's and Neumann's addition theorems, Numer. Algorithms. 72 (2016) 91–106. https://doi.org/10.1007/s11075-015-0035-1.

[31] A.W. Leissa, Vibration of Shells, American Institute of Physics, 1993.

[32] M.P. Norton, D.G. Karczub, Fundamentals of Noise and Vibration Analysis for Engineers, 2nd ed., Cambridge University Press, Cambridge, 2003. https://doi.org/10.1017/CBO9781139163927.

[33] R.F. Keltie, The effect of hydrostatic pressure fields on the structural and acoustic response of cylindrical shells, J. Acoust. Soc. Am. 79 (1986) 595–603. https://doi.org/10.1121/1.393755.

[34] C.T.F. Ross, Pressure vessels under external pressure - Statics and dynamics, Elsevier Applied Science, London, 1990.